Relationships among Cloud Occurrence Frequency, Overlap, and Effective Thickness Derived from CALIPSO and CloudSat Merged Cloud Vertical Profiles

Seiji Kato,[1] Sunny Sun-Mack,[2] Walter F. Miller,[2] Fred G. Rose,[2] Yan Chen,[2]

Patrick Minnis,[1] and Bruce A. Wielicki[1]

Yan Chen, Science Systems & Applications Inc. Hampton, Virginia 23681-2199, USA. (Yuan.Chen@nasa.gov)

Seiji Kato, Climate Science Branch, NASA Langley Research Center Hampton, Virginia 23681-2199, USA. (Seiji.Kato@nasa.gov)

Walter F. Miller, Science Systems & Applications Inc. Hampton, Virginia 23681-2199, USA. (Walter.F.Miller@nasa.gov)

Patrick Minnis, Climate Science Branch, NASA Langley Research Center Hampton, Virginia 23681-2199, USA. (P.Minnis@nasa.gov)

Fred G. Rose, Science Systems & Applications Inc. Hampton, Virginia 23681-2199, USA. (Fred.G.Rose@nasa.gov)

Sunny Sun-Mack, Science Systems & Applications Inc. Hampton, Virginia 23681-2199, USA. (Szedung.Sun-Mack-1@nasa.gov)

Bruce A. Wielicki, Climate Science Branch, NASA Langley Research Center Hampton, Virginia 23681-2199, USA. (Bruce.A.Wielicki@nasa.gov)

Abstract. A cloud frequency of occurrence matrix is generated using merged cloud vertical profiles derived from the satellite-borne Cloud-Aerosol Lidar with Orthogonal Polarization (CALIOP) and Cloud Profiling Radar (CPR). The matrix contains vertical profiles of cloud occurrence frequency as a function of the uppermost cloud top. It is shown that the cloud fraction and uppermost cloud top vertical profiles can be related by a cloud overlap matrix when the correlation length of cloud occurrence, which is interpreted as an effective cloud thickness, is introduced. The underlying assumption in establishing the above relation is that cloud overlap approaches random overlap with increasing distance separating cloud layers and that the probability of deviating from random overlap decreases exponentially with distance. One month of Cloud-Aerosol Lidar and Infrared Pathfinder Satellite Observation (CALIPSO) and CloudSat data (July 2006) support these assumptions, although the correlation length sometimes increases with separation distance when the cloud top height is large. The data also show that the correlation length depends on cloud top hight and the maximum occurs when the cloud top height is 8 to 10 km. The cloud correlation length is equivalent to the

[1]Climate Science Branch, NASA Langley Research Center, Hampton, Virginia, USA.

[2]Science Systems and Applications, Inc., Hampton, Virginia, USA.

decorrelation distance introduced by *Hogan and Illingworth* [2000] when cloud fractions of both layers in a two-cloud layer system are the same. The simple relationships derived in this study can be used to estimate the TOA irradiance difference caused by cloud fraction, uppermost cloud top, and cloud thickness vertical profile differences.

1. Introduction

An accurate characterization of the vertical profiles of cloud properties is critical for calculating the radiative flux divergence within and at the top of the atmosphere. For example, *Barker et al.* [2003] demonstrated that, for a given vertical distribution of liquid water content, changing the cloud overlap conditions can alter the zonal annual mean top-of-atmosphere (TOA) cloud radiative effect by up to 50 Wm^{-2}. In addition, estimating the cloud base height accurately is important for surface radiation budget computations especially in polar regions. For example, simply changing the base height of an optically thick cloud from 5 km to 1 km in a subarctic standard atmosphere increases the downward longwave irradiance by nearly 10%. In addition to the importance of cloud overlap to radiation, cloud overlap affects precipitation parameterizations in general circulation models (GCMs). If precipitation falls through clouds, collision and coalescence need to be considered but for precipitation falling through cloud-free air, evaporation needs to be considered [*Jakob and Klein*, 2000].

Multi-layer cloud information cannot be retrieved from passive sensor data except when a thin layer overlaps optically thick warm clouds [e.g., *Chang and Li*, 2005] or a moderately thick ice clouds occurs over a water cloud over a water surface [*Minnis et al.*, 2007]. In addition, multi-layer clouds sometimes cause a cloud height retrieval error that depends on specific algorithm and cloud properties [*Naud et al.* 2007]. Additionally, retrievals of total cloud water path tend to be biased when an ice cloud overlaps a liquid water cloud [*Minnis et al.*, 2007]. New active sensors, however, are now providing multi-layer cloud information lacking in previous satellite measurements. The Cloud-Aerosol Lidar and Infrared Pathfinder Satellite Observation (CALIPSO) [*Winker et al.* 2007] satellite and CloudSat [*Stephens et al.* 2002] provide detailed data on the vertical profile of clouds from the Tropics to polar regions. The CALIPSO Cloud-Aerosol Lidar with Orthogonal Polarization (CALIOP) [*Winker et al.* 2007] and CloudSat Cloud Profiling Radar (CPR) [Im et al. 2005] identify multi-layered cloud top and base heights that are not easily detected with passive sensors.

In earlier studies, *Hogan and Illingworth* [2000] derived cloud overlap statistics from ground-based radar data and introduced the variable α that linearly combines the random and maximum cloud overlap. They assumed that α decreases exponentially as the separation between two cloud layers increases and defined the e-folding distance (or decorrelation distance). *Wang and Dessler* [2006] used 20 days of Ice, Cloud,and land Elevation Satellite (ICESat) data over the Tropics to show that a third of boundary layer clouds overlap nearly randomly with cirrus clouds. *Mace and Benson-Troth* [2002] extended the work of *Hogan and Illingworth* [2000] and derived seasonal and regional variations of α and its e-folding distance using ground-based Atmospheric Radiation Measurement (ARM) radar data taken at four different sites. *Barker* [2008b] derived α from 2 months of CPR and CALIOP combined data and found that, over Southern Great Plains (SGP) ARM site, the decorrelation distance is consistent with that reported by *Mace and Benson-Troth* [2002]. Willén et al. (2005) interpreted the decorrelation distance as an indirect measure of the cloud thickness. A mathematical relationship between the decorrelation distance and cloud thickness for a two-layer cloud system is given by *Astin and Di Girolamo* [2006].

In this study, we form a cloud frequency of occurrence matrix and develop a cloud overlap matrix to quantify vertical cloud profiles derived from CALIPSO and CloudSat.

Observations from CALIPSO and CloudSat are closely matching in time as a part of the a-train constellation [*Stephens et al.* 2002]. The accuracy of overlapping CALIOP and CPR footprints in the coordination of satellite pointing is discussed in, for example, Stephens et al. [2008] and Mace et al. [2009]. Cloud profiles from either CALIPSO or CloudSat alone are not enough to provide a complete picture of cloud vertical structure; the CPR tends to miss thin clouds composed of small cloud particles (the minimum detection is -30 dBZ, *Stephens et al.* [2008]) and the CALIOP signal is completely attenuated by optically thick clouds (optical thickness greater than about 3). A first step in using multi-layer cloud information from CALIOP and CPR is, therefore, to merge cloud vertical profiles (hereinafter merged cloud profiles) derived independently from these two instruments.

The primary purpose of this paper is to describe a tool for quantitatively analyzing cloud vertical profiles in order to assess their impact on radiation. We treat complicated and highly variable vertical cloud structures statistically and characterize them using a simple expression that uses only a few variables. Our approach to quantitatively evaluate vertical cloud profiles and overlap is different than that introduced by *Hogan and Illingworth* [2000]. Merged cloud profiles are sorted to form a simple cloud frequency of occurrence matrix. We then develop a cloud overlap matrix that is composed of a set of equations relating vertical profiles of the cloud fraction exposed to space, cloud fraction and cloud physical thickness. These observed profiles determine the macroscopic structure of clouds that affects radiation. The relationships among cloud fraction, uppermost cloud top vertical profiles, and cloud thickness also provide a physical interpretation of the decorrelation distance that is used in GCMs to parameterize cloud overlap.

Typically, the effect of cloud overlap on radiation is estimated by computing TOA irradiance changes with various cloud overlap assumptions using a GCM generated cloud fields (e.g. *Barker et al.* [2003]). While these computations provide an accurate sensitivity, they do not provide the explicit dependence of the TOA irradiance. As a result, when cloud profiles are altered, the detailed computation needs to be redone. As we demonstrate in the discussion section, simple relationships derived in this study can be used to understand sensitivities of the TOA irradiance and provide the TOA irradiance dependence to cloud profile explicitly. Note that only correlations of cloud mask are considered in this paper and correlations of liquid or ice water, treated by *Hogan and Illingworth* [2003], are not considered here.

Once cloud profiles from CALIOP and CPR are merged and cloud vertical profiles are obtained, the impact of cloud structures on the irradiance profiles can be assessed by comparing the irradiances computed with merged cloud profiles to those computed with simple single-layer clouds. Clouds and the Earth's Radiant Energy System (CERES) data products show that TOA irradiances derived from CERES instrument radiance measurements is accurate when they are sorted by cloud type (Loeb et al. 2005, Loeb et al. 2007) and averaged over a month or longer period. The data have been analyzed to understand clouds-radiation interaction by cloud type (e.g. Xu et al. 2004). CALIPSO and CloudSat provide multi-layer cloud and aerosol layers, which further improves the understanding of cloud and aerosol processes affecting radiation. For this reason, we collocate merged cloud profiles with footprints of the CERES FM-3 instrument on *Aqua*. Another purpose of this paper is to describe the process used to merge CALIOP and CPR derived cloud profiles within a CERES footprint. Although this study does not use CERES-derived irradiances, this paper includes descriptions of the collocation process with CERES footprints in Section 2 because the process is interwoven with the CALIOP and CPR cloud profile merging process.

Once merged cloud profiles are collocated with CERES footprints, radiative effects at the surface and in the atmosphere are examined using irradiance vertical profiles computed by a radiative transfer model. With this goal, cloud information is maintained at the original CALIOP and CPR resolutions as much as possible while collocating and merging them into CERES footprints. This allows the independent column approximation to be properly applied in computing the irradiance profile. A plane parallel assumption in modeling irradiances over a 20 km CERES footprint is sometimes violated due to the horizontal photon transport through the boundary. However, a 20 km scale allows us to analyze the irradiance by cloud type. When computed irradiances at a 20 km resolution are averaged over a year, they agree with surface observations to within 10% (Kato et al. 2008).

In this paper, Section 2 describes the process combining CALIOP and CPR derived cloud profiles and the process merging those profiles with the CERES footprints. Section 3 introduces the cloud frequency of occurrence matrix and derives a cloud overlap matrix that is composed of a set of equations relating the cloud fraction, uppermost cloud top fraction, and cloud thickness. It also discusses the relation of our approach to the decorrelation distance concept introduced by *Hogan and Illingworth* [2000]. In section 4, we utilize the relationships determined from the cloud overlap matrix and perform a simple sensitivity study of TOA irradiance to cloud overlap.

2. CALIPSO and CloudSat combined cloud profile

In this study, we use the version 2 Vertical Feature Mask (VFM) CALIPSO data product and 2B-CLDCLASS CloudSat data product. The VFM product provides a cloud and aerosol mask with a 0.333-km horizontal resolution below 8.2 km altitude and a 1-km horizontal resolution above 8.2 km [*Winker et al.,* 2007]. The VFM vertical resolution is 30 m below and 60 m above the altitude of 8.2 km [*Winker et al.* 2007]. The CLDCLASS product based on CPR reflectivity provides a cloud mask with a 1.4-km cross-track horizontal resolution, a 1.8 km along-track resolution, and a uniform vertical resolution of 240 m [*Stephens et al.* 2008].

To take advantage of both the CALIOP and CPR instruments, the VFM and CLDCLASS profiles are collocated on 1-km × 1-km grids simply using latitude and longitude. When none of the center of CPR profiles falls within a 1-km × 1-km grid box, the closest CPR profile from the center of a grid box is collocated instead of interpolating two close CPR profiles. As a result, each 1-km × 1-km grid box contains 3 CALIPSO profiles with data above 8.2 km replicated and one CPR profile. The combined cloud profiles are then collocated with CERES footprints, which are approximately 20 km in size. Note that the actual point spread function of the CERES instrument (FM-3) is approximately 35 km because the response time causes a widening and skewing [*Smith*, 1994]. The point spread function size of 35 km, which is used in this study, covers 95% energy detected by the CERES instrument. CALIOP and CPR derived cloud vertical profiles are merged based on the cloud top and base heights (hereinafter vertical profile merging process), and if necessary, merged cloud profiles that fall within a CERES instrument footprint are grouped together (hereinafter vertical profile grouping process). In the following subsections, we describe these two vertical profile merging and grouping processes.

2.1. Vertical profile merging process

Every 1-km by 1-km grid box contains one CloudSat and three VFM vertical profiles. Each CALIPSO-derived cloud profile is compared with a collocated CloudSat-derived cloud profile for merging. Cloud top and base heights for the grid box are determined using the strategy described in Table 1. Because the CPR range resolution is 485 m, even though CPR acquires samples approximately every 240 m [*Tanelli et al.* 2008], the CALIOP and CPR derived cloud boundaries need to differ more than 480 m to be considered as distinctly different boundaries. Therefore, when the CPR identifies a cloud boundary that is more than 480 m away from the CALIOP-derived cloud boundary (i.e. CALIOP did not detect clouds in the height range between CPR-detected cloud top and base), the cloud boundary is inserted into the CALIOP derived cloud profile. When CALIOP signal is not completely attenuated, cloud bases are taken from the CALIOP data (Table 1) to avoid the influence of precipitation on the cloud radar [e.g. *Clothiaux et al.* 2000]. As a result of the above cloud boundary merging strategy, the merged cloud profiles are primarily based on CALIOP derived cloud profiles, except when the signal is completely attenuated. About 85% of cloud tops and 77% of cloud bases of the merged profiles are derived from CALIOP data.

2.2. Vertical profile grouping process

The number of unique cloud profiles within the CERES point spread function can be as many as 50 (Figure 1a). We determined the maximum number of unique groups allowed within a CERES footprint to be 16 and a maximum of 6 layers is to be allowed within a group for reasons described in this subsection. For cases when the number of unique groups exceeded sixteen, we combined profiles with nearly the same cloud top and base heights. The cloud grouping process is summarized by a schematic diagram in Figure 2.

Figure 1b shows the cloud fraction covered by unique cloud groups greater than the cloud group number indicated in the legend. The cloud group number having the largest cloud fraction over a CERES footprint is 1 and the largest cloud number is assigned to the cloud group having the smallest cloud fraction. As shown in the discussion section, the cloud fraction error caused by a cloud overlap error needs to be smaller than 0.09 in order for the TOA irradiance error to be smaller than 3 Wm^{-2}. According to Figure 1b, the sum of cloud fractions from unique cloud groups greater than fourteen is smaller than 0.09 most of the time. The distribution of cloud boundary vertical distances that were both kept at the original height and altered by the cloud grouping process is shown in Figure 1c. Nearly 80% of cloud boundaries were not altered. Among boundaries that were altered, 60% of those were altered less than 250 m and 87% of those were altered less than 500 m. Relatively large changes in the cumulative distribution around 240 and 480 m are caused by changing CPR derived cloud boundaries. Figures 1b and 1c show, therefore, cloud boundaries were altered less than 500 m in cloud profiles covers approximately 1% of the area by keeping 16 unique cloud groups. Because of this, the cloud grouping process predominately changes the order of occurrence of cloud profiles within approximately a 35 km length of the ground track.

Even before the algorithm reduces it to the maximum of 6, the number of vertical layers in a profile is less than 6 for most of the merged profiles (Figure 3). For the month of data analyzed here, 99.68 % of merged profiles contain 6 or fewer vertical cloud layers. To check the effect on the grouping process to the cloud fraction, the cloud fraction difference compared with those from original CALIPSO and CPR derived cloud profiles is shown in Figure 4. The zonal cloud fraction difference is less than 0.002 (Figure 4b), the cloud fraction difference is less than 0.005 at all 200 m vertical layers (Figure 4c), and the difference in the cloud fraction exposed to space is less than 0.0005 (Figure 4d). These results show, therefore, imposing the size of a CERES footprint as a domain to form cloud groups does not degrade the original cloud vertical profile information observed by CALIOP and CPR.

3. Cloud Frequency of Occurrence Matrix

To form a cloud frequency of occurrence matrix, the merged cloud vertical profiles are sorted by the uppermost cloud top height z_{top} with a bin size of 200 m counting the number of cloud occurrences below the uppermost cloud top. This produces a cloud occurrence 2D histogram having columns separated by the highest cloud top z_{top} and rows containing the vertical profile of cloud occurrence for a given uppermost cloud top. The element defined by the column i and row j contains the number of cloud occurrences in the layer j when the uppermost cloud top height $z_{top,i}$ is at the layer i. The probability of cloud occurrence in the layer j with the uppermost cloud top at the layer i is

$$P(z_j, z_{top,i}) = n_{ji}/N, \tag{1}$$

where n_{ji} is the number of occurrences in row j and column i, N is the total number of profiles, including cloud-free profiles. Note that the cloud layer index starts from the surface and increases with altitude so that

$$n_{ji} \geq 0 \quad when \quad j \leq i, \quad and \quad n_{ji} = 0, \quad when \quad j > i, \tag{2}$$

resulting in a cloud frequency of occurrence matrix that is an upper triangular matrix. This differs from the cloud overlap matrix defined by Willén et al. (2005), matrix elements in which are cloud fraction exposed to space by a two-cloud layer system. In our approach, the uppermost cloud layers, which are the diagonal elements of the cloud frequency of occurrence matrix, are the clouds exposed to space.

The sum of all of the uppermost cloud layers computed over a region for a given period defines the mean cloud fraction

$$C = \frac{\sum_{i=1}^{m} n_{ii}}{N} = \sum_{i=1}^{m} P(z_i, z_{top,i}), \tag{3}$$

where m is the total number of vertical layers and $P(z_i, z_{top,i})$ is the probability of cloud occurrence in the uppermost layer i. The conditional probability that clouds are present in the layer j when the uppermost cloud top height is $z_{top,i}$ is

$$P(z_j|z_{top,i}) = \frac{P(z_j, z_{top,i})}{P(z_i, z_{top,i})}, \tag{4}$$

and $P(z_i|z_{top,i}) = 1$. The frequency of cloud occurrence in the layer j with any uppermost cloud top heights (i.e. the probability of cloud occurrence in layer j regardless of cloud occurrence above) is

$$P(z_j) = \frac{\sum_{i=j}^{m} n_{ji}}{N} = \sum_{i=j}^{m} P(z_j, z_{top,i}). \tag{5}$$

Note that the probability of cloud occurrence depends on the vertical depth of the bin (Appendix A). In this study, we use a bin size that is sufficiently smaller than the thickness of cloud in order to minimize the effect.

With the above definitions, the random overlap probability of a cloud in the layer j and layer i is $P(z_j)P(z_i)$. The random overlap probability between clouds at the layer j and a uppermost cloud top layer at $z_{top,i}$ is $P(z_j)P(z_i, z_{top,i})$. Therefore, the conditional probability of random overlap of clouds in the layer j with an uppermost cloud top is at $z_{top,i}$ is,

$$P_{rdm}(z_j|z_{top,i}) = P(z_j)P(z_i, z_{top,i})/P(z_i, z_{top,i}) = P(z_j). \tag{6}$$

We further divide the conditional probability $P(z_j|z_{top,i})$ into two terms,

$$P(z_j|z_{top,i}) = \frac{P(z_j, z_{top,i})}{P(z_i, z_{top,i})} = P_{rdm}(z_j|z_{top,i}) + \Delta P(z_j|z_{top,i}), \tag{7}$$

where $P_{rdm}(z_j|z_{top,i})$ is the probability of random overlap defined in Eq. 6, and ΔP is the deviation from random overlap. Therefore,

$$\Delta P(z_j|z_{top,i}) = \frac{P(z_j, z_{top,i})}{P(z_i, z_{top,i})} - P(z_j). \tag{8}$$

When $j = i$,

$$\Delta P(z_i|z_{top,i}) = 1 - P(z_i). \tag{9}$$

Similar to the assumption made in earlier studies (e.g. *Hogan and Illingworth* [2000]), when $j \leq i$, we assume that ΔP decreases exponentially with vertical distance,

$$\Delta P(z_j|z_{top,i}) \approx [1 - P(z_i)] \exp(-\Delta z_{ji}/D_i), \tag{10}$$

where Δz_{ji} is the distance from the uppermost cloud top i to the layer j, $z_{top,i} - z_j$, and D is the e-folding distance or correlation length of cloud occurrence. Hence, D is the vertical distance over which the probability of cloud occurrence deviates from random overlap by a factor of e. Note that the subscript of D indicates that the correlation length is a function of the uppermost cloud top height. If there is no physical process connecting two layers, we would expect that the clouds in those two layers overlap randomly. Therefore, the e-folding distance D_i can be interpreted as the distance over which the physical process controlling the cloud formation falls off by a factor of e. As pointed out by *Astin and Di Girolamo* [2006], therefore, we can interpret D_i as the effective thickness of cloud.

When $\Delta z = 0$ and Eq. 10 is substituted in Eq. 7, $P(z_i|z_{top,i}) = 1$, provided $P_{rdm}(z_i|z_{top,i}) = P(z_i)$. Hence, the conditional probability of overlap with itself is 1. Therefore $1 - P(z_i)$ in Eq. 10 is the conditional probability of cloud in layer i overlapping the uppermost cloud top i that deviates from random overlap.

Equation A5 in Appendix A suggests that the necessary condition to establish the relationship of exponential decay is that the vertical bin size must be small compared to D. For simplicity, we fix the bin size to 200 m throughout the atmosphere in this study.

Note that our bin size is larger than the 90 m used by *Mace and Benson-Troth* [2002]. We expect, however, that D derived from data does not depend on the bin size very much so long as the bin size is smaller than D. A study by *Wang et al.* [2000] indicates that the mode thickness of cloud layers is about 500 m.

Given the uppermost layer at the layer i, the probability of cloud occurrence at the layer j is,

$$P(z_j|z_{top,i}) = P(z_j) + [1 - P(z_i)]\exp[-(z_i - z_j)/D_i]. \tag{11}$$

When we multiply Eq. 11 by $P(z_i, z_{top,i})$ and sum up all uppermost cloud top layers above the jth layer(i.e. from $i = j$ to m), then

$$P(z_j) = \sum_{i=j}^{m} P(z_i, z_{top,i})P(z_j) + \sum_{i=j}^{m} P(z_i, z_{top,i})[1 - P(z_i)]\exp\left[-(z_i - z_j)/D_i\right], \tag{12}$$

because $P(z_j|z_{top,i})P(z_i, z_{top,i}) = P(z_j, z_{top,i})$ and $\sum_{i=j}^{m} P(z_j, z_{top,i}) = P(z_j)$. The cloud occurrence in the layer j is, therefore,

$$P(z_j)[1 - \sum_{i=j+1}^{m} P(z_i, z_{top,i})] = P(z_j, z_{top,j}) + \sum_{i=j+1}^{m} P(z_i, z_{top,i})[1 - P(z_i)]e^{-(z_i - z_j)/D_i}, \tag{13}$$

where m is the highest cloud layer detected by CALIOP and the CPR. Equation 13 for all layers can be expressed as a matrix operation

$$\mathbf{P} = \mathbf{DT}, \tag{14}$$

where

$$\mathbf{P} = [P(z_1), P(z_2) \cdots P(z_m)]^T, \tag{15}$$

$$\mathbf{T} = [P(z_1, z_{top,1}), P(z_2, z_{top,2}) \cdots P(z_n, z_{top,n})]^T, \tag{16}$$

$$\mathbf{D} = \begin{pmatrix} \frac{1}{1-\sum_{i=2}^{m} P(z_i,z_{top,i})} & \frac{[1-P(z_2)]e^{-\frac{z_2-z_1}{D_2}}}{1-\sum_{i=2}^{m} P(z_i,z_{top,i})} & \cdots & \frac{[1-P(z_{m-1})]e^{-\frac{z_{m-1}-z_1}{D_{m-1}}}}{1-\sum_{i=2}^{m} P(z_i,z_{top,i})} & \frac{[1-P(z_m)]e^{-\frac{z_m-z_1}{D_m}}}{1-\sum_{i=2}^{m} P(z_i,z_{top,i})} \\ 0 & \frac{1}{1-\sum_{i=3}^{m} P(z_i,z_{top,i})} & \cdots & \frac{[1-P(z_{m-1})]e^{-\frac{z_{m-1}-z_2}{D_{m-1}}}}{1-\sum_{i=3}^{m} P(z_i,z_{top,i})} & \frac{[1-P(z_m)]e^{-\frac{z_m-z_2}{D_m}}}{1-\sum_{i=3}^{m} P(z_i,z_{top,i})} \\ \vdots & \vdots & \ddots & \vdots & \vdots \\ 0 & 0 & \cdots & \frac{1}{1-\sum_{i=n}^{m} P(z_i,z_{top,i})} & \frac{[1-P(z_m)]e^{-\frac{z_m-z_{n-1}}{D_m}}}{1-\sum_{i=n}^{m} P(z_i,z_{top,i})} \\ 0 & 0 & \cdots & 0 & 1 \end{pmatrix} \tag{17}$$

and superscript T denotes the transpose of the matrix. In Eqs. 15, 16, and 17, m is the number of cloud layers, n is the number of the uppermost cloud layer, and $n = m$. Equation 14 relates the cloud fraction profile, the uppermost cloud top profile (i.e. the cloud fraction exposed to space) and cloud effective thickness. When the cloud vertical correlation length as a function of uppermost cloud top height is known, therefore, vertical cloud fraction and uppermost cloud top profile can be related. Because **D** is an upper triangular matrix, if either the cloud fraction or the uppermost cloud top vertical profile is known, it can be solved for the other unknown profile provided the correlation length is known. To solve the set of equations, the highest layer is set to,

$$P(z_m, z_{top,m}) = P(z_m). \tag{18}$$

In earlier studies (*Hogan and Illingworth* [2000]; *Bergman and Rasch* [2002]; *Barker* [2008]) the cloud fraction exposed to space C_{kl} for a two-cloud layer system, layers k and l, is written as

$$C_{kl} = C_{rdm} - \alpha(C_{rdm} - C_{max}), \quad (19)$$

where C_{rdm} and C_{max} are, respectively, the cloud fraction given by the random and maximum overlap assumptions, α is the parameter that linearly combines C_{rdm} and C_{max} [Hogan and Illingworth 2000]. This can be written with the notation used here as

$$C_{kl} = P(z_l) + P(z_k) - P(z_k)P(z_l) - \alpha P(z_l)\left[\frac{min[P(z_k), P(z_l)]}{P(z_l)} - P(z_k)\right], \quad (20)$$

where the layer l is the upper layer, $min[P(z_k), P(z_l)]$ is equal to the smaller value between $P(z_k)$ and $P(z_l)$ and $\alpha = e^{\frac{-(z_l - z_k)}{\Delta z_0}}$.

For a two-layer cloud system of k and l, the total cloud fraction is the sum of cloud fractions in the upper and lower layers exposed to space. Using the correlation length, the cloud fraction exposed to space is, therefore,

$$C_{kl} = P(z_l) + P(z_k) - P(z_k)P(z_l) - P(z_l)[1 - P(z_l)]e^{-\frac{z_l - z_k}{D_k}}. \quad (21)$$

The last term on the right side in Eqs. 19, 20, and 21 reduces the cloud fraction exposed to space from that given by the random overlap assumption. Cloud fractions exposed to space computed by Eqs. 20 and 21 differ for an arbitrary pair of two-layer cloud fractions when the distance between the two layers is small. The cloud fractions given by Eqs. 20 and 21 are equal when $P(z_l) = P(z_k)$, so when $\alpha = e^{-(z_l - z_k)/\Delta z_0}$, our correlation length D

is equivalent to the decorrelation distance Δz_0. *Astin and Di Girolamo* [2006] derived the same conclusion although they have an additional requirement that the variances of the cloud fraction for both layers must be small compared with the respective cloud fraction. It appears that the requirement of small variances is needed when the cloud fraction over a region is observed for multiple time periods. Note that even when the distance between the two layers approaches zero, C_{kl} by Eq. 21 does not approach the upper layer cloud fraction unless the cloud fractions in the upper and lower layers are the same. When the distance between the cloud layers is small and there is no strong meteorological boundary such as a strong temperature inversion between two layers, the difference in the cloud fraction is also small with the difference approaching zero as the distance decreases due to the finite thickness of clouds. In practice, therefore, C_{kl} in Eq. 21 approaches C_{max} when the distance is small compared with the correlation length.

4. Discussion

Figures 5 and 6 show, respectively, the vertical profile of cloud fraction $P(z)$ and $\Delta P(z|z_{top})$ (Eqs. 5 and 8) derived from 1 month of data (July 2006) for 6 latitude bands. Note that, in Figure 5, a large cloud fraction occurs above the tropopause over Antarctica because these clouds at 10 to 14 km are difficult to classify as polar stratospheric clouds for two reasons (D. Winker and M.Pitt personal communication 2009). It is sometimes difficult to identify the exact height of tropopause over Antarctica and these clouds sometimes extends from the troposphere into the stratosphere. A monotonic decrease of $\Delta P(z|z_{top})$ with the distance from the uppermost cloud top is seen in Figure 6. For large distances, especially in the southern hemisphere tropics, $\Delta P(z|z_{top})$ is sometimes negative. One possible reason for this is that the CALIOP signal is sometimes completely attenuated while the CPR misses low-level clouds implying that low-level clouds occur less often than random overlap when mid and high level clouds are present. To understand the occurrence of clouds missed by both CALIOP and CPR, i.e. clouds occur below the level of complete attenuation of the CALIOP signal and are undetected by CPR, Figure 7 shows the frequency of occurrence of cloud base undetected by CPR when CALIOP signal was completely attenuated (dotted line). The frequency of occurrence of undetected cloud base height varies between 10 to 20% depending on latitude (Figure 7).

When deriving Eq. 13, it was assumed that ΔP in Eq. 8 decreases exponentially with distance from the uppermost cloud top. Figure 8 shows ΔP as a function of distance from the uppermost cloud top for selected uppermost cloud top heights. For the figure, ΔP is derived from Eq. 8, i.e. $\Delta P = P(z_j|z_{top,i}) - P(z_j)$. The slope of the line shown in Figure 8 is the inverse of the correlation length. Figure 8 indicates that ΔP decreases nearly exponentially with distance from the uppermost cloud top for moderate separation distances. Note that ΔP at a distance of 0 km is $1 - P(z_i)$ given by Eq. 9, where $P(z_i)$ is the cloud fraction in the layer (at the distance of 0 km). When the line is nearly horizontal, the conditional probability, the cloud occurrence in the layer j for the cloud top at the layer i, is nearly constant if cloud fraction below the layer j is nearly constant. Therefore, a large correlation length, evident as a smaller slope in Figure 8, might be an indication of precipitation, although frequently occurring convective clouds cannot be ruled out as a possible cause. An example of this smaller slope is seen at distance between 4 and 7 km from the uppermost cloud top for the 8.9 km case in the left-hand panel. A small slope near the cloud top might be caused by the finite thickness of clouds i.e. the existence of a minimum cloud thickness. When the line is nearly vertical below the layer j, clouds below the layer j overlap nearly randomly with clouds having a cloud top at layer i.

Because the inverse of the slopes of the lines shown in Figure 8 is the correlation length, the correlation length as a function of the uppermost cloud top height can be derived through linear regressions. However, Figure 8 indicates that the slope is not necessarily constant throughout the atmospheric column for a given uppermost cloud top for the various possible reasons discussed above. Therefore, applying a linear regression between the uppermost cloud top and the surface can lead to a biased estimate if increasing the correlation length with separation distance is due to precipitation. To reduce the error, we compute the slope using a 1.2-km moving window and average all slopes so that a constant slope extending over the largest vertical length is given the greatest weight. Because we expect that clouds overlap randomly when the distance from the uppermost cloud top is large and we wish to avoid the effect of possible precipitation, we only sample with the moving window over the distance equivalent to 50% of the uppermost cloud top height starting from the uppermost cloud top. As expected, the correlation length, which is the effective cloud thickness, increases with uppermost cloud top height (Figure 9). The correlation length reaches a maximum when the uppermost cloud top height is 8 to 10 km. When the uppermost cloud top height is above 8 km, the correlation length gradually decreases with height in the polar regions and tropics. This might be caused by frequently occurring thin cirrus. The correlation length in the Tropics does not differ from midlatitude values, probably because very thick convective clouds does not occur frequently even in the tropics compared with the occurrence of other cloud types [*Dong et al.* 2008]. This also suggests that the correlation length depends on the size of domain over which the cloud overlap matrix is formed. If the domain is small and deep convective clouds occur frequently in the domain, the correlation length would be larger. The correlation length of clouds present over the Antarctic around 9 km is larger than that over other regions, suggesting the presence of clouds with a large vertical extent during polar night. This is consistent with the existence of clouds over Antarctica that extend from the troposphere into the stratosphere.

To understand the sensitivity of the correlation length to the values we chose to derive the slope, we changed the size of the moving window and height range for the sampling. Doubling the size of the moving window to 2.4 km changes the correlation length less than 10% for clouds with the top height exceeding ≈5 km. The difference can be nearly 50% for clouds with the top height below 5 km because the physical thickens of clouds is often smaller than 2.4 km. In addition, we changed the vertical sampling distance by the moving window to the distance equivalent to 25% of the cloud top height. When 25% of the uppermost cloud top height is sampled, the correlation length tends to be smaller than the values derived from 50% of the uppermost cloud top height (Figure 9). Although we need to further refine the method adopted here to derive the slope, the changes induced by these two values are small. They are less than the distance (≈ 1.3 km) that changes the TOA shortwave irradiance by an equivalent amount due to neglecting the height dependence of the decorrelation length, as discussed later in this section.

4.1. Sensitivity study using cloud overlap matrix

The correlation length derived here is related to the decorrelation length introduced by *Hogan and Illingworth* [2000] as indicated by Eqs. 20 and 21. They are not exactly the same but the decorrelation distance, a property used within GCMs, coincides with the correlation distance of clouds defined in this paper when the cloud fraction of the two layers are equal. Therefore, this result provides a physical interpretation of the decorrelation distance and its relationship to cloud fraction, which should give some insight into how it is derived and how it can be approximated. For example, *Barker* [2008a] speculated that the decorrelation distance depends on altitude. As expected, results in Figure 9 indicate that the decorrelation distance depends on the cloud top height, because, clearly, the cloud thickness depends on cloud type.

The height dependence of the decorrelation distance is sometimes neglected when parameterizing the cloud overlap [*Barker* 2008a, *Barker and Räisänen* 2005]. The error in the zonal and monthly mean TOA shortwave irradiance caused by neglecting the height dependence of the decorrelation distance in computing the TOA shortwave irradiance is less than 3 Wm^{-2} [*Barker* 2008a]. If it is assumed that the height dependence of the decorrelation distance has a negligible impact on a cloud overlap parameterization used for computing the TOA irradiance, the following criterion can be employed to determine whether the process described here to obtain the correlation length can be used to extract cloud overlap. Forming the cloud overlap matrix and deriving the correlation length have an advantage as opposed to the decorrelation distance because the process is straightforward compared to the method used for deriving decorrelation distance. When the difference between the decorrelation distance and the correlation length gives a smaller TOA irradiance change compared with that caused by the height dependence of the decorrelation distance, therefore, the cloud correlation length introduced here might be used as the decorrelation distance for a cloud overlap parameterization.

To obtain a rough estimate of the sensitivity of the TOA reflected shortwave irradiance to the correlation length, we use Eq. 13 and take a derivative with respect to D,

$$\frac{\partial P(z_k, z_{top,k})}{\partial D_l} = -\frac{z_l - z_k}{D_l^2} P(z_l, z_{top,l})[1 - P(z_l)]e^{-(z_l - z_k)/D_l}, \qquad (22)$$

where the layer l is the upper layer. The actual cloud fraction in a layer depends on the vertical depth of the layer and size of domain, but we use $P(z_l, z_{top,l}) = P(z_l) \approx 0.25$ in the following sensitivity study based on Figure 5 to demonstrate the impact of cloud overlap to the TOA shortwave irradiance. If we further assume that $D_l = 2$ km, and $z_l - z_k = 2$ km, a 1.0 km error in D_l gives about a 0.034 cloud fraction error in $P(z_k, z_{top,k})$. If we use a typical value of $\approx -40\text{Wm}^{-2}$ for zonal mean TOA shortwave cloud forcing in the Tropics and 0.6 for a zonal mean cloud fraction exposed to space (e.g. *Kato et al.* [2008]), changing cloud fraction by 0.1 gives a difference of about 7 Wm^{-2} at the TOA. A rough estimate of the maximum error in the correlation length that gives an equivalent TOA shortwave change caused by neglecting height dependence of decorrelation distance ($\approx 3\text{Wm}^{-2}$) is, therefore, about 1.3 km.

Earlier studies indicate that the variability of TOA shortwave irradiance is mostly caused by the variability of the cloud fraction exposed to space [*Loeb et al.* 2007, *Kato* 2009]. The relationships among the uppermost cloud top, correlation length, and cloud fraction suggests that the cloud fraction exposed to space changes due to the correlation length and the cloud fraction in the vertical layers. In the above two-layer system, the effective cloud thickness D_l determines whether the cloud in layer k vertically extends from the layer l or the clouds exposed to space to become a part of a cloud extending from the uppermost cloud layer k. The sensitivity of the cloud fraction exposed to space to the correlation length is largest when layers k and l are separated by the distance D_l, which is apparent from Eq. 13.

Earlier studies (e.g. *Barker et al.* [2003]) further show that the cloud fraction exposed to space largely depends on cloud overlap assumption. The change in TOA shortwave irradiance caused by switching from the random to the maximum cloud overlap assumption depends on the errors in the correlation length and the cloud fraction. If errors in the correlation length and the cloud fraction in the vertical layers are large, adopting a proper cloud overlap assumption may not significantly improve TOA irradiance estimates. The change in the cloud fraction exposed to space due to changing from the random to the maximum/random cloud overlap assumption in a two-layer cloud system is the last term on the right side of Eq. 21,

$$\Delta P(z_k, z_{top,l}) = P(z_l)[1 - P(z_l)]e^{\frac{-(z_l - z_k)}{D_k}}. \tag{23}$$

When the distance of the separation is 2 km, for example, the cloud fraction exposed to space changes approximately 0.07, which changes the TOA irradiance by 4.8 Wm^{-2} if we assume a 0.1 cloud fraction change causes a 7 Wm^{-2} cloud forcing change. For a two-layer cloud system, the ratio of the cloud fraction change given by this expression to the cloud fraction change due to the error in the correlation length given by Eq. 21 is, therefore,

$$\frac{\Delta P}{\frac{\partial C_{kl}}{\partial D_l}\Delta D_l} = \frac{D_l^2}{(z_l - z_k)\Delta D_l}, \tag{24}$$

where ΔP is the cloud fraction difference between random and maximum/random overlap, and ΔD_l is the error in the correlation length. The characterization of cloud overlap can be improved by including the correlation length when the ratio given by Eq. 24 is grater than unity. When we use $D_l = 2$ km, adopting the correlation length should improve the estimate of the cloud fraction exposed to space for a two-layer cloud system separated by less than 3 km when the error in the correlation length is 1.3 km.

The sensitivity of the cloud fraction exposed to space due to the error in the cloud fraction is

$$\frac{\partial P(z_k, z_{top,k})}{\partial P(z_k)} = 1 - \sum_{i=k+1}^{m} P(z_i, z_{top,i}). \tag{25}$$

The second term on the right is the cloud fraction exposed to space above the layer k. Comparing Eq. 25 to the difference in the cloud fraction exposed to space between the random and maximum / random overlap Eq. 23, we find that when

$$\Delta P(z_k) < P(z_l) e^{\frac{-(z_l - z_k)}{D_l}}, \tag{26}$$

the error in the cloud fraction exposed to space due to the error in the cloud fraction $\Delta P(z_k)$ is smaller than $\Delta P(z_k, z_{top,l})$. Therefore, the improvement of the TOA irradiance estimate caused by adopting a proper cloud overlap parameterization is large if the upper layer cloud fraction $P(z_l)$ is large. Give the cloud fraction in GCMs has an error, therefore, this result suggests that regions in which the cloud overlap needs to improve in GCMs are regions where high and mid level cloud fraction is large. When we use $P(z_l) \approx 0.25$, $D_l = 2$ km, and $z_l = z_k = 2$ km, we find that the cloud fraction error must be smaller than

0.09 to improve the TOA irradiance. As the distance separating cloud layers increases, the cloud fraction exposed to space is more affected by the cloud fraction error because clouds tends to overlap randomly.

The above simple sensitivity study utilizes the cloud overlap matrix derived in this study. The matrix relates the cloud fraction exposed to space, which passive sensors provide, and the vertical cloud fraction profile, which GCMs compute, using the height dependent correlation length. Imposing observed cloud overlap to GCMs may or may not improve the TOA irradiance computation depending on the cloud fraction profile and cloud fraction error in the model. Table 2 provides a summary of the sensitivity study results using a two-layer cloud system when the upper layer cloud fraction is 0.25.

5. Conclusions

We combined vertical cloud profiles from CALIPSO and CloudSat to utilize the strength of each instrument to quantitatively understand vertical cloud profile. We introduced the cloud frequency of occurrence matrix that contains the vertical cloud profile as a function of the uppermost cloud top. Assuming that cloud overlap approaches random overlap as the distance between the two cloud layers increases and defining the e-folding distance of the cloud occurrence probability deviating from the random overlap, we formed a cloud overlap matrix and showed that the uppermost cloud top and the cloud fraction vertical profiles can be related. The e-folding distance, or correlation length, is interpreted as the effective cloud thickness. Cloud vertical profiles derived from the CALIOP and CPR show that the cloud fraction deviating from the random overlap in layers below the uppermost cloud layer nearly decays exponentially with the distance separating the two layers. The maximum correlation length occurs between 8 to 10 km for all 6 regions. However, the data also show that the correlation length is not necessarily constant throughout the atmospheric column for a given uppermost cloud top height. When the uppermost cloud top height is large, the correlation length sometimes increases as the separation distance increases. The large correlation length might be caused by precipitation or frequently occurring convective clouds. The correlation length estimated here using a moving window that samples the upper part of clouds minimizes the effect of precipitation and convective clouds. While the relationships among three profiles are independent of the domain size, the actual values of the correlation length, cloud fraction, and cloud fraction exposed to space depend on the size of domain used to derive them.

In a two-layer cloud system, the correlation length is equivalent to the decorrelation distance introduced by *Hogan and Illingworth* [2003] when the upper and lower cloud fractions are the same. Relationships among cloud occurrence frequency, overlap, and effective thickness provide some insights valuable for deriving GCM cloud overlap parameterizations. When the error in the correlation length is less than 1.3 km in a two-layer cloud system with the upper layer cloud fraction of 0.25, the error in the TOA shortwave flux is less than 3 $\mathrm{Wm^{-2}}$, which is equivalent to the error neglecting the height dependence of the decorrelation distance. The improvement of cloud fraction exposed to space occurs when the separation of a two-layer cloud system is 3 km when the correlation length error is 1.3 km. Adopting the correlation length improves TOA irradiances if the lower layer cloud fraction error for a two-layer cloud system is less than 0.09.

As demonstrated in the paper, CALIPSO and CloudSat data provide the cloud fraction vertical profile and vertical profile of cloud fraction exposed to space. Once the cloud overlap matrix is formed, the correlation length can be derived from it. In addition, not only validations of cloud overlap parameterizations used in GCMS, a full comparison of cloud fields generated by cloud models utilizing a finer spatial resolution than that in GCMs is possible. Simple relationships derived in this paper provide an estimate of TOA irradiance changes caused by the cloud field difference without running a radiative transfer model. This would be an advantage of forming the cloud overlap as opposed to directly deriving decorrelation distance from active sensor data to characterize cloud overlap.

Appendix A: The effect of the vertical bin size

If we assume that the conditional probability of cloud occurrence decreases exponentially with the distance from the uppermost cloud top to the layer j, the probability density function $p(z_j|z_{top,i})$ is

$$p(z_j|z_{top,i}) = \frac{1}{D_i} e^{-z_{ji}/D_i}. \tag{A1}$$

The probability of cloud occurrence in the uppermost layer of Δz_i thickness is

$$P(z_i|z_{top,i}) = \int_0^{\Delta z_i} \frac{1}{D_i} e^{-z/D_i} dz = 1 - e^{-\Delta z_i/D_i}. \tag{A2}$$

When $\Delta z_i/D_i \ll 1$, $P(z_i|z_{top,i}) \approx \Delta z_i/D_i$. The probability of cloud occurrence in the layer j the thickness of which is Δz_j and distance from the uppermost cloud top layer i z_{ji} is

$$P(z_j|z_{top,i}) = \int_{z_{ji}-\Delta z_j/2}^{z_{ji}+\Delta z_j/2} \frac{1}{D_i} e^{-z/D_i} dz = e^{\frac{-z_{ji}}{D_i}} \left(e^{\frac{\Delta z_j}{2D_i}} - e^{\frac{-\Delta z_j}{2D_i}} \right). \tag{A3}$$

The conditional probability then becomes

$$\frac{P(z_j|z_{top,i})}{P(z_i|z_{top,i})} = \frac{e^{\frac{-z_{ji}}{D_i}}\left(e^{\frac{\Delta z_j}{2D_i}} - e^{\frac{-\Delta z_j}{2D_i}}\right)}{1 - e^{\frac{-\Delta z_i}{D_i}}}. \quad \text{(A4)}$$

When $\Delta z_i/D_i \ll 1$, $\Delta z_j/D_i \ll 1$, and $\Delta z_i = \Delta z_j$ the conditional probability is

$$\frac{P(z_j|z_{top,i})}{P(z_i|z_{top,i})} \approx e^{-z_{ji}/D_i}. \quad \text{(A5)}$$

Acknowledgments. We thank Drs. David Winker, Charles Trepte, Mark Vaughan, Gerald Mace, Roger Marchand, Larry Di Girolamo, Robert Holz, Lazaros Oreopoulos, Toshihisa Matsui, and one anonymous reviewer for helpful discussions and comments. The work was supported by the NASA Science Mission Directorate through the NASA Energy Water Cycle Study (NEWS) project.

References

Astin, I, and L. Di Girolamo, (2006), The relationship between α and the cross-correlation of cloud fraction, *Q. J. R. Meteorol. Soc.*, 132, 2475-2478.

Barker, H. W. (2008a), Representing cloud overlap with an effective decorrelation length: An assessment using CloudSat and CALIPSO data *J. Geophys. Res.*, 113, D24205, dio:10.1029/2008JD010391.

Barker, H. W, (2008b), Overlap of fractional cloud for radiation calculation in GCMs: A global analysis using CloudSat and CALIPSO data, *J. Geophys. Res.*, 113, D00A01, dio:10.1029/2007JD009677.

Barker, H. W. and P. Räisänen, (2005), Radiative sensitivities for cloud structural properties that are unresolved by conventional GCMs *J. Q. R. Meteorol. Soc.*, 131, 3103-3122.

Barker, H. W., and co-authors, (2003), Assessing 1D atmospheric solar radiative transfer models: interpretation and handling of unresolved clouds, *J. Climate*, 16, 2676-2699.

Chang, F.-L., and Z. Li, (2005), A new method for detection of cirrus-overlapping-water clouds and determination of their optical properties. *J. Atmos. Sci.*, 62, 3993-4009.

Clothiaux, E. E., and co-authors, (2000), Objective Determination of Cloud Heights and Radar reflectivities Using a Combination of Active Remote Sensors at the ARM CART Sites, *J. Appl. Meteorol.*, 39, 645-665.

Dong, X., B. A. Wielicki, B. Xi, Y. Hu, G. G. Mace, S. Benson, F. Rose, S. Kato, T. Charlock, and P. Minnis, (2008), Using observations of deep convective systems to constrain atmospheric column absorption of solar radiation in the optically thick limit, *J. Geophys. Res.*, 113, D10206, doi:10.1029/2007JD009769.

Hogan, R. J., and A. J. Illingworth, (2003), Parameterizing ice cloud inhomogeneity and he overlap of inhomogeneities using cloud radar data, *J. Atmos. Sci.,*, 60, 756-767.

Hogan, R. J., and A. J. Illingworth, (2000), Deriving cloud overlap statistics from radar, *Q. J. R. Meteorol. Soc.*, 126, 2903-2909.

Im, E. S. L. Durden, and C. Wu (2005), Clod profiling radar fro the CloudSat mission, *IEEE Trans. Aerosp. Electron. Syst.*, 20, 15-18, doi:10.1109/MAES.2005.1581095.

Jakob, C., and S. A. Klein, (2000), A parameterization of the effect of cloud and precipitation overlap for use in general-circulation models, Q. J. R. Meteorol. Soc., 126, 2525-2544.

Kato, S, F. G. Rose, D. A. Rutan, and T. P. Charlock, (2008), Cloud effects on the meridional atmospheric energy budget estimated from Cloud and the Earth's Radiant Energy System (CERES) data, *J. Climate*, 21, 4223-4241.

Kato, S. (2009), Interannual variability of the global radiation budget, *J. Climate*, 22, 4893-4907.

Loeb, N. G. B. A. Wielicki, F. G. Rose, and D. R. Doelling (2007), Variability in global top-of-atmosphere radiation between 2000 and 2005, *Geophys Res. Lett*, 34, L03704, doi:10.1029/2006GL028196.

Loeb, N. G., S. Kato, K. Loukachine, and N. Manlo-Smith, (2005) Angular Distribution Models for Top-of-Atmosphere Radiative Flux Estimation from the Clouds and the Earth's Radiant Energy System Instrument on the Terra Satellite. Part I: Methodology *J. Atmos. Ocean. Technol.*, 338-351.

Loeb, N. G., S. Kato, K. Loukachine, N. Manlo-Smith, and D. R. Doelling, (2007) Angular Distribution Models for Top-of-Atmosphere Radiative Flux Estimation from the Clouds and the Earth's Radiant Energy System Instrument on the Terra Satellite. Part II: Validation *J. Atmos. Ocean. Technol.*, 564-584.

Mace, G. G., and S. Benson-Troth, (2002), Cloud-layer overlap characteristics derived from long-term cloud radar data, *J. Climate*, 15, 2505-2515.

Mace, G. G., Q. Zhang, M. Vaughan, R. Marchand, G. Stephens, C. Trepte, and D. Winker, (2009), A description of hydrometer layer occurrence statistics derived from the first year of merged CloudSat and CALIPSO data, *J. Geophys. Res.*, 114, D00A26, doi:10.1029/2007JD009755.

Minnis, P., J. Huang, B. Lin, Y. Yi, R. F. Arduini, T.-F. Fan, J. K. Ayers, and G. G. Mace (2007), Ice cloud properties in ice-over-water cloud systems using TRMM VIRS and TMI data, *J. Geophys. Res.*, 112, D06206, doi:10.1029/2006JD007626.

Naud, C. M. B. A. Baum. M. Pavolonis, A. Heidinger, R. Frey, and H. Zhang, (2007), Comparison of MISR and MODIS cloud-top heights in the presence of cloud overlap, *Remote Sens. Environ.*, 107, 200-210.

Smith, G. L. (1994), Effects of time response on the point spread function of a scanning radiometer, *Appl Opt.*, 30, 7031-7037.

Stephens, G. L. and co-authors, (2002), The CloudSat mission and a-train, *Bull. Amer. Meteor. Soc.*, 83, 1771-1790.

Stephens, G. L., and co-authors, (2008), CloudSat mission: performance and early science after the first year of operation, *J. Geophys. Res.*, 113, D00A18, doi:10.1029/2008JD009982.

Wang, J., W. B. Rossow, Y. Zhang, (2000), Cloud vertical structure and its variations from 20-yr global rawinsonde dataset, *J. Climate*, 13, 3041-3056.

Wang, L., and A. E. Dessler, (2006), Instantaneous cloud overlap statistics in the tropical area revealed by ICESat/GLAS data, *Geophys. Res. Lett.*, 33, L15804, doi:10.1029/205GL024350.

Willén, Ulrika, S. Crewell, H. K. Baltink, and O. Sievers, (2005), Assessing model predicted vertical cloud structure and cloud overlap with radar and lidar ceilometer observations for the Baltex Bridge Campaign, *Atmos. Res.*, 75, 227-255.

Winker, D. M., W. H. Hunt, and M. J. Mcgill, (2007), Initial performance assessment of CALIOP, *Geophys. Res. Lett.*, 34, L19803, doi:10.1029/2007GL030135.

Xu, K.-M., T. Wong, B. A. Wielicki, L. Parker, Z. A. Eitzen, (2005), Statistical analyses of satellite cloud object data for large ensemble evaluation of cloud models. Part I: Methodology and preliminary results, *J. Climate*, 18, 2497-2514.

Table 1. Cloud mask merging strategy

Cloud boundary	CALIOP	CPR	Merged boundary
Top	Detected	Detected	Higher cloud top
Top	Detected	Undetected	CALIOP cloud top
Top	Undetected	Detected	CPR cloud top
Base	Not completely attenuated	Undetected	CALIOP cloud base
Base	Not completely attenuated	Detected	CALIOP cloud base
Base	Completely attenuated	Detected	CPR cloud base
Base	Completely attenuated	Undetected	CALIOP lowest unattenuated base

Table 2. Summary of sensitivity study[1] (cloud fraction is ≈ 0.25)

Variables	Value	Result
Correlation length error	1.3 km	causes 3 Wm^{-2} TOA SW flux error (Eq. 22)
Cloud layer vertical distance contributing to improve TOA flux	3.0 km	when the correlation distance error is 1.3 km (Eq. 23)
TOA SW irradiance change switching from random to random overlap	4.8 Wm^{-2}	when $D_l = 2$ km, $z_l - z_k = 2$
Maximum lower-level cloud fraction error to improve TOA flux	0.09	when $D_l = 2$ km, $z_l - z_k = 2$ km in Eq. 25

[1] The irradiance change is computed with an assumption of 0.1 cloud fraction change causes 7 Wm^{-2} irradiance change.

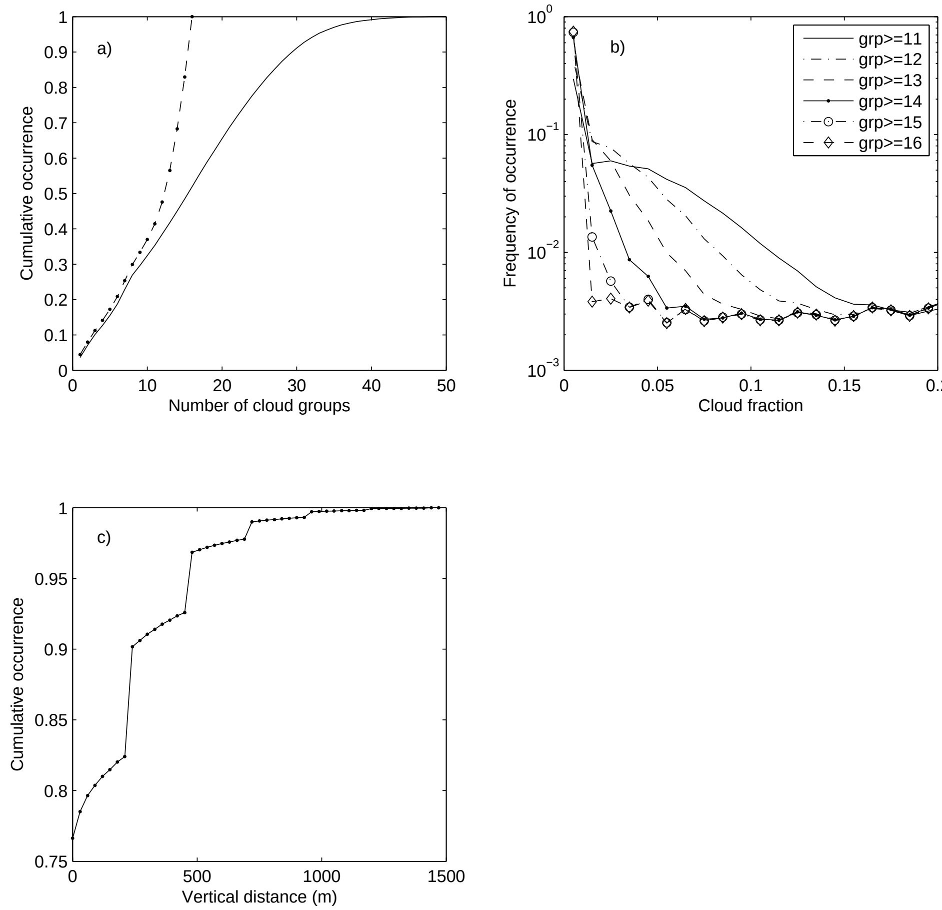

Figure 1. (a) Cumulative distribution of the number of cloud groups in a CERES footprint. The solid line indicates the cumulative distribution of the actual number of unique profiles and the dashed line indicates the cumulative distribution after reducing to the maximum of 16 groups in a CERES footprint. (b) Histogram of cloud fraction covered by cloud groups greater than or equal to the cloud group number indicated in the legend. The cloud group number having the largest cloud fraction over a CERES footprint is 1 and the largest cloud number is assigned to the cloud group having the smallest cloud fraction. (c) Cumulative distribution of cloud boundary vertical distances altered by the cloud grouping process. The occurrence at the vertical distance equal to 0 is for boundaries kept at the original height.

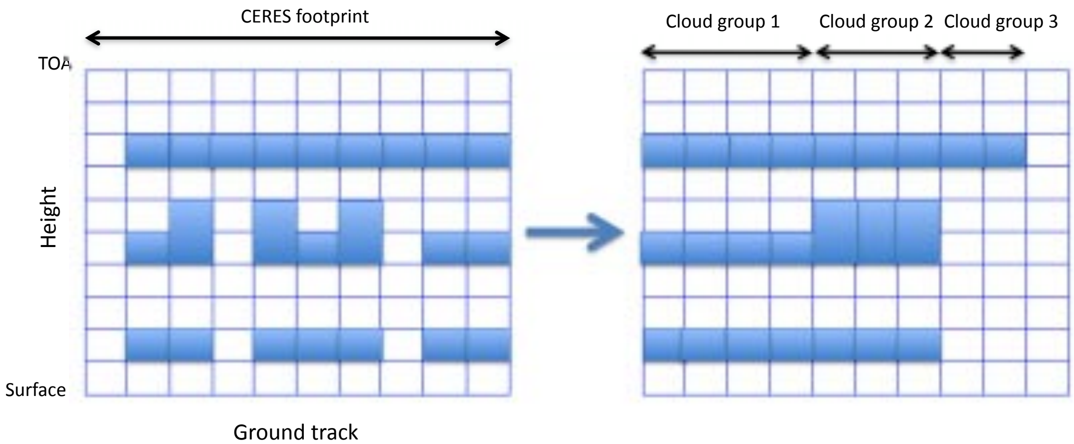

Figure 2. Schematic of the cloud grouping process. Cloud profiles that occur within a CERES footprint and have the same cloud boundary heights are grouped together. The group number of 1 is assigned to the cloud group having the largest cloud fraction over a CERES footprint.

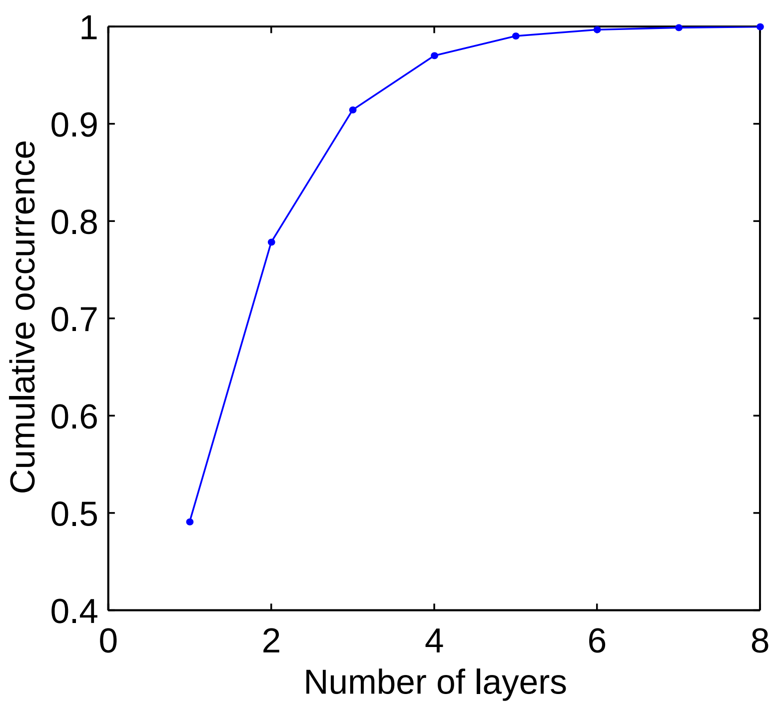

Figure 3. Cumulative occurrence of the number of vertical cloud layers in a merged CALIPSO-CloudSat cloud profile. Up to 6 layers were kept in merged cloud vertical profiles.

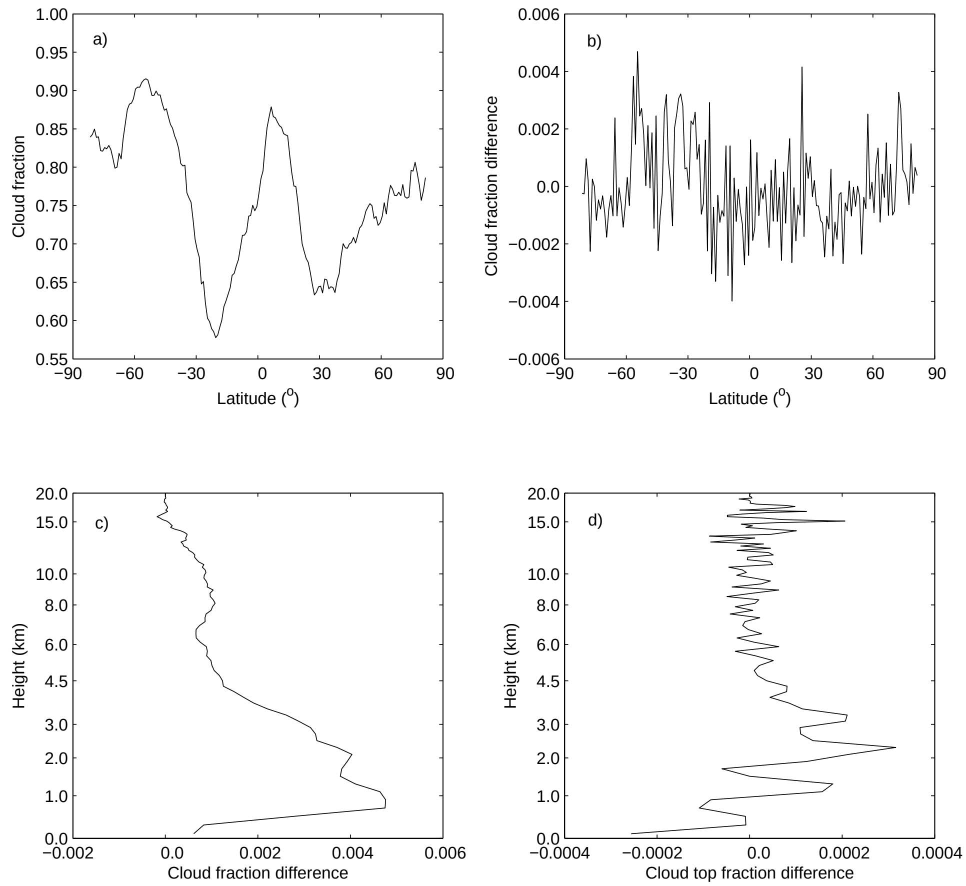

Figure 4. (a) Cloud fraction exposed to space derived from CALIPSO-CloudSat merged cloud profiles before the grouping process as a function of latitude. (b) The difference of the zonal mean cloud fraction exposed to space, (c) the difference in the cloud fraction vertical profile within 200 m vertical layers, and (d) the difference in the uppermost cloud top fraction vertical profile within 200 m vertical layers. All differences are computed by subtracting the values before the grouping process from the value after the process using global July 2006 data.

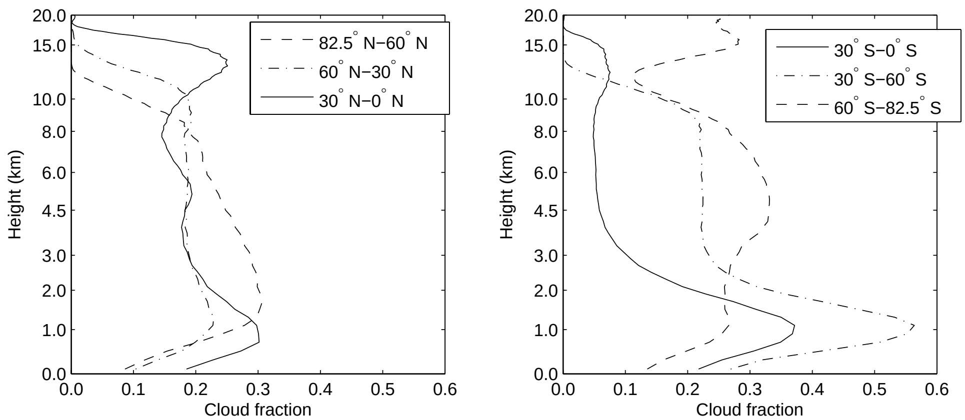

Figure 5. Cloud faction vertical profile derived from CALIOP and CPR merged cloud profiles computed with a 200 m vertical resolution for July 2006. left) northern hemisphere and right) southern hemisphere.

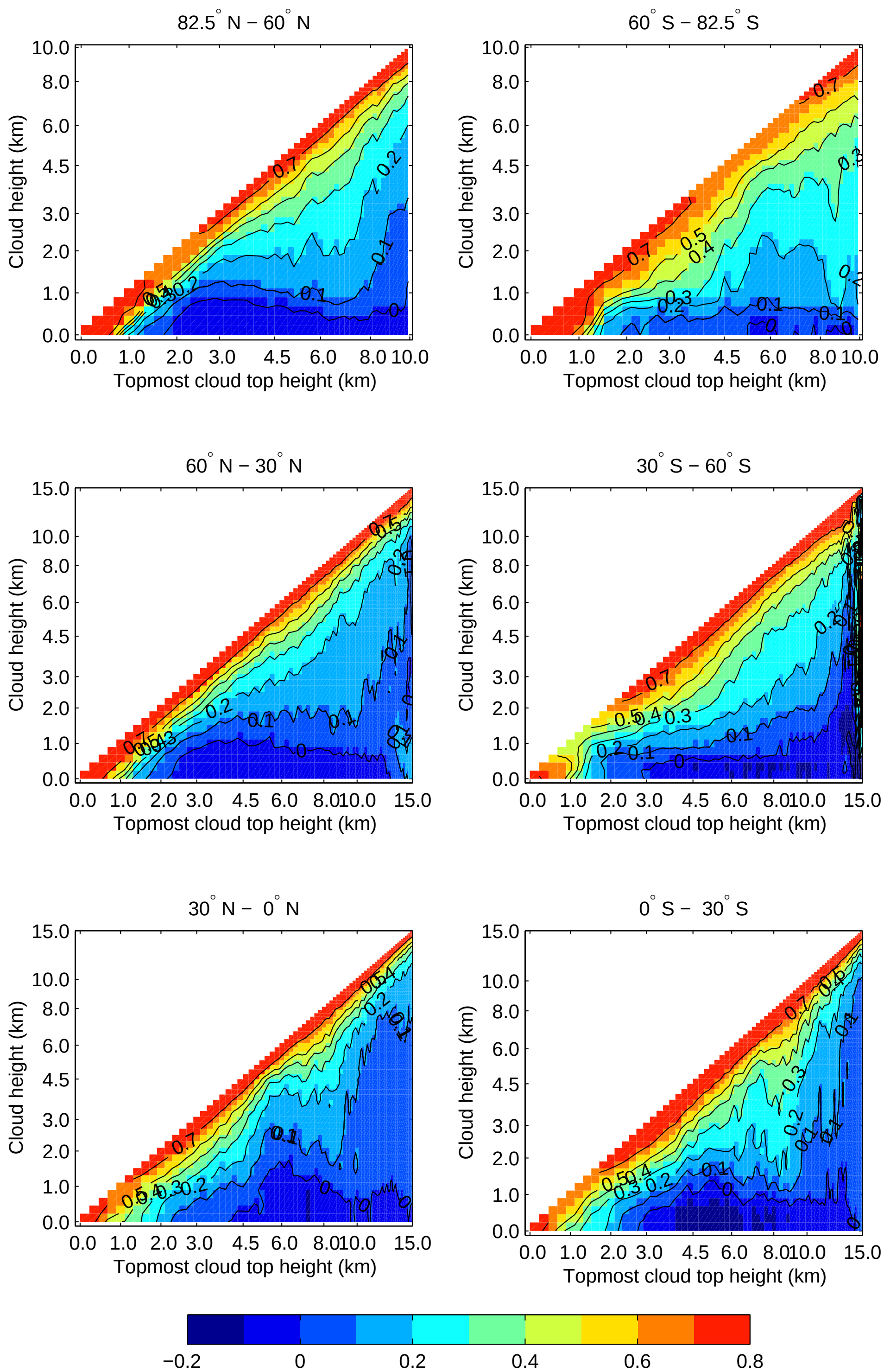

Figure 6. Deviation from the random overlap ΔP defined in by Eq. 8 as a function of uppermost cloud top height for 6 different regions. These are 2D histograms of the conditional probability of cloud occurrence in 200 m vertical layers deviating from the random overlap probability sorted by uppermost cloud top height. Cloud vertical profiles are derived from July 2006 CALIOP and CPR data.

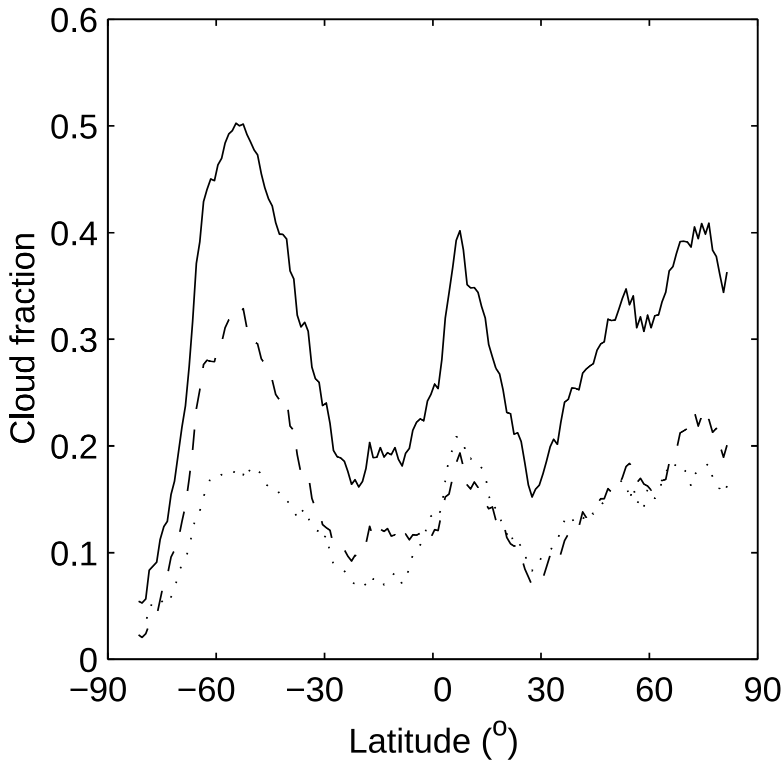

Figure 7. Fraction of clouds that attenuate CALIOP signal completely (solid line). Dashed line indicates the fraction of clouds having a cloud base detected by the CPR below the height where the CALIOP signal is completely attenuated. The dotted line indicates the fraction of clouds the base of which was not detected by CALIOP and CPR, i.e. the difference between solid and dashed lines.

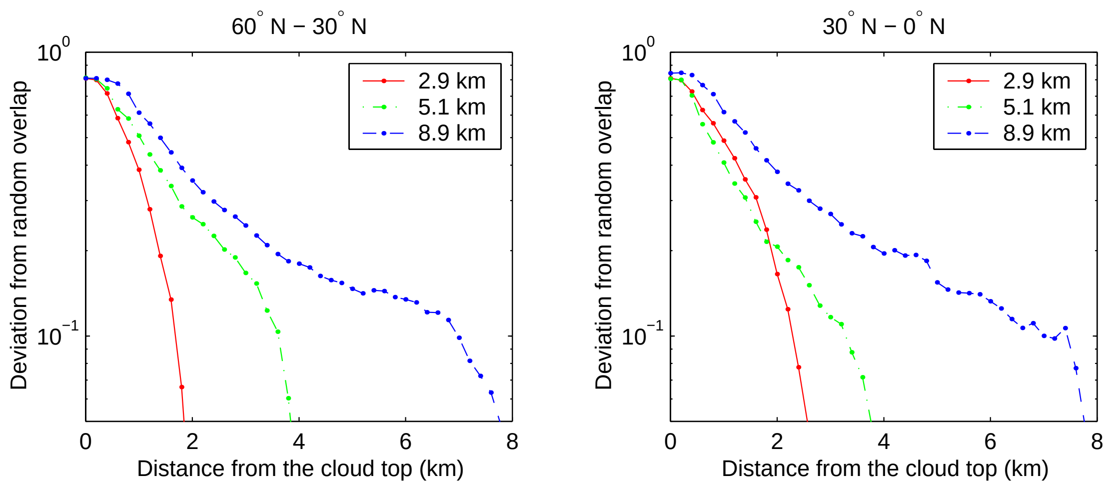

Figure 8. Deviation from the random overlap ΔP that is plotted in Figure 6 as a function of distance from the uppermost cloud top for three uppermost cloud top heights.

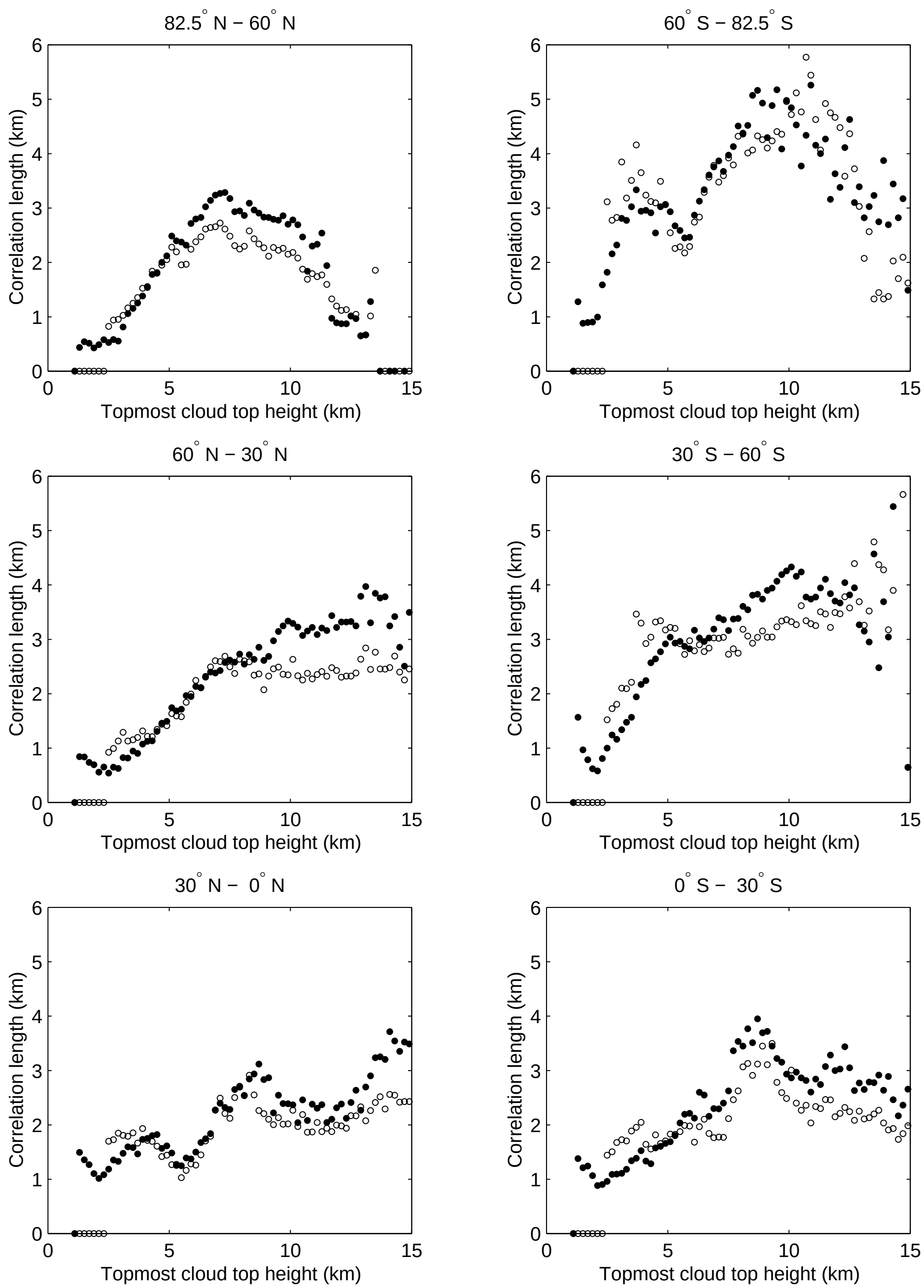

Figure 9. Correlation length derived from one month (July 2006) of CALIOP and CPR data as a function of uppermost cloud top height for 6 different regions. Sensitivity of correlation length to assumptions in the deriving algorithm is shown by the small difference between open and closed circles, which vary the fraction of the atmosphere used; the distance of $0.25z_{top}$ (open circles) or $0.5z_{top}$ (closed circles) from the uppermost cloud top z_{top}.